Dynamics of Oscillating Erythrocyte Doublets after Electrofusion

Martin Baumann
Institut für Physiologie der RWTH Aachen, 52057 Aachen, Germany

ABSTRACT Erythrocytes were electrofused with multiple rectangular voltage pulses to show an oscillatory movement, divided into swell phases and pump events. During each swell phase, which lasted from 0.5 s to more than 180 s, the fused cells' (doublets') volume increased by colloid osmotic swelling, and the membrane area was expanded until rupture. Membrane rupture initiated the pump event, where the doublets' volume and membrane area decreased with an almost exponential time course and time constants between 2 ms and 8 ms. Simultaneously, a portion of cytosolic hemoglobin solution was ejected into extracellular space ("jet"). Pump event time constants and swell phase durations decreased with rising chamber temperature, indicating that both parts of the oscillatory movements were determined by physical properties of membrane and liquids. Relative volume change developments express a gradual loss of membrane elasticity during the oscillation, decreasing the elastic forces stored in the membrane. Evidence is given that the first rupture causes a weakening of the membrane at the rupture site. Heat treatment up to 45°C had a negligible effect on swell times, pump time constants, and relative volume changes. A heat treatment of 50°C prevented oscillatory movements. The rupture location accorded with theories of potential induced membrane electropermeabilization.

INTRODUCTION

Cell fusion applications

In vitro fusion of biological cells is a widely used method for cell manipulation. Some of the applications involve determination of electrical and mechanical membrane properties (Zimmermann and Vienken, 1982; Zimmermann, 1982), detection of lateral diffusion processes in cell membranes (Song et al., 1991; Sowers 1990), and understanding the biomechanics of virus-to-cell fusion (Akkaş, 1984; Sowers, 1992). Among the methods used for the initiation of the fusion process, the following types serve as important examples: cell fusion based on the presence of viruses (Akkaş, 1984; Morris et al., 1989; Hernandez et al., 1996), laser light-based initiation of cell fusion (Steubing et al., 1991), fusion based on chemicals like polyethylene glycol (Lentz, 1994), and electrical initiation of cell fusion processes (see, e.g., Zimmermann and Vienken, 1982; Zimmermann, 1982). The advantages of the latter method are its independence of cell type, its transient effect, and the ability to trigger experimental data acquisition apparatus (Sowers, 1992). Cell fusion not only can be used to determine the kinetics and the mechanics of the fusion process itself; it is also useful for initiating colloid osmotic swelling and the oscillation cycle (Baumann and Sowers, 1996a). Still not totally clear is the behavior of the spectrin cytoskeleton at the fusion initiation and during the fusion process. Experimental data of this work provide a hypothesis for the role of spectrin during the fusion process.

Received for publication 30 September 1998 and in final form 30 July 1999.

Address reprint requests to Dr. Martin Baumann, Institut für Physiologie, Klinikum der RWTH Aachen, Pauwelsstrasse 30, 52057 Aachen, Germany. Tel.: 49-241-80-88823; Fax: 49-241-8888-434; E-mail: martin@physiology.rwth-aachen.de.

0006-3495/99/11/2602/10 $2.00

Cell fusion and membrane mechanics

In this project, cell fusion is used to initiate the oscillation mechanism that occurs with fused erythrocytes and to examine physical membrane parameters by the evaluation of the oscillation dynamics. The fusion process itself is paid minor attention.

In the process of cell fusion the membranes of the involved cells undergo several consecutive steps, which have been investigated in the past in detail with erythrocytes. At first, membrane contact or *bilayer adherence* is inevitable for fusion initiation. It can be accessed via a high concentration of cells in the buffer, causing multiple accidental membrane contacts, or via dielectrophoresis (Pohl, 1978), causing intended single or multiple membrane contacts, like a pearl chain formation. The electrical fusion initiation itself is mostly applied after bilayer adherence has taken place, the so-called *normal protocol* or *contact-first protocol*. However, fusion initiation can be applied before physical membrane contact is established; this is known as *inverse protocol* or as *pulse-first protocol* with a reduced fusion yield (Montane et al., 1990; Sowers, 1987; Teissié and Rols, 1993; Wu et al., 1992). After these two steps, *bilayer joining* takes place, in which the two cell membranes fuse (Song et al., 1991). Thus the size of the visible fusion area or fusion zone increases and its kinetics can be taken as a measurement of fusion velocity (Baumann and Sowers, 1996b; Sowers, 1995). Only after this step can cell fusion start (Knutton and Pasternak, 1979), or the fusion process ceases and results in an *irreversible membrane contact.* One result of the cell fusion can be a *flat diaphragm fusion,* in which a persistent membrane layer remains visible in light microscopical images. This layer possesses from three to more than 10 pores with a minimum diameter of 0.1 μm (Chernomordik and Sowers, 1991) and thus reduces the

mixture of the endoplasmic volumes of the two cells involved. Another result of cell fusion results in the creation of a real syncytium, called *open lumen fusion* (Sowers et al., 1994; Sowers, 1995).

Normal fusion kinetics result in a continuous, almost exponential increase in the fusion zone diameter (Wu et al., 1994b), which is the projection of the fusion zone. This motion is parallel to a continuous increase in both cells' diameters and a reduction in the distance between the center points of the two cells. Its kinetics are ruled by the influence of the spectrin network (Sowers, 1995; Wu et al., 1994a,b).

DOUBLET OSCILLATION

Phenomenology

The oscillation movement of fused cells is a repetitive movement, which can be seen with electrofused erythrocytes (Glaser and Donath, 1987). This paper focuses on oscillations of two fused cells, called a *doublet.* Necessary terminology is given in Fig. 1. Higher clusters of fused cells ($n > 2$) can also show oscillatory movements (Baumann and Sowers, 1996a). After the fusion event, the fusion product initially exhibits normal fusion kinetics, i.e., a shape change from the 8-configuration (also known as the *hourglass configuration*; Knutton and Pasternak, 1979) to the O-configuration (Fig. 2, 0th swell phase). At a certain ratio of the doublet's length to width, it undergoes a rapid shape change toward an earlier configuration (Fig. 2, first pump event), from that on starting anew with a phase of normal fusion kinetics (Fig. 2, first swell phase). The rapid shape change, or pump event, can be absent—when the doublet only shows normal fusion kinetics—or occur up to 15 times or more (Baumann, 1998; Baumann and Sowers, 1996a), depending on experimental conditions. The exact time when the pump event occurs is unpredictable. The pump event itself is accompanied by an ejection of cytoplasmic solution into the extracellular space (a *jet*) and is visible not only with doublets (Baumann, 1998; Baumann and Grebe, 1998) but also with unfused swollen erythrocytes (Marsden et al., 1981; Zade-Oppen, 1998). The jet is observable at least for first pump events in light microscopic images, drawn schematically in Fig. 1.

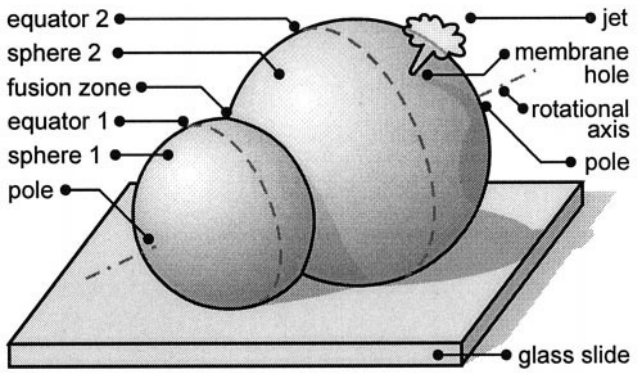

FIGURE 1 Schematic drawing of two fused cells on a glass slide. The configuration consists of two intersected spheres, with a pointed conjunction at the fusion zone. Because this configuration has a rotational symmetry, two poles and two equators can be defined as shown.

The amplitude of the shape changes between two pump events decreases with ongoing oscillations (Baumann, 1998). The pump event itself is a fast motion with exponential changes in the geometry and time constants τ between $\tau = 2$ ms and $\tau = 8$ ms. The swell phase is about three orders of magnitude slower than the pump event and shows almost linear geometrical changes with time intervals of $t = 0.5$ s up to more than 180 s. The duration of two consecutive swell phases does not become continuously shorter or longer, but almost always the last swell phases are shorter than the first (Baumann and Grebe, 1998). The described phenomenology suggests that the doublet's oscillatory movement can be regarded as a system that exhibits nonlinear oscillations (Schmid-Schönbein, 1996).

A doublet can be accurately described as two intersected spheres (Fig. 1) that do not necessarily have the same size (Fig. 3). Because of the rotational symmetry, calculation of membrane surface area and doublet volume becomes possible with measurements of two-dimensional microscopic images. Fig. 3 shows a sequence of images with a time resolution of 5 s taken from an oscillating doublet.

Explanation for the oscillatory movement

After the fusion-initiating voltage pulse is applied to the erythrocytes, cells fuse and continue to show an osmotically induced volume increase (the swell phase). Parallel to this, the doublet's membrane is expanded (see Fig. 7 *B*) and thus stores elastic energy. After the maximum tolerated membrane area expansion is reached, the membrane shows a single rupture, which creates a hole of multiple macromolecular size. Through this hole, cytoplasmic volume is ejected into extracellular space, driven by the elastic energy that was previously stored and now is converted into the kinetic energy of the jet. The jet causes a volume decrease of the doublet (see Fig. 7 *A*) and closes afterward, allowing the cycle of swell phase and pump events to start over.

MATERIALS AND METHODS

Materials and blood treatment

Human blood was drawn from healthy volunteers by finger prick and diluted in phosphate-buffered saline buffer (0.2 g/liter KCl, 0.2 g/liter KH_2PO_4, 8 g/liter NaCl, and 1.15 g/liter Na_2HPO_4) to match a hematocrit of 2.6%. Samples were stored at 0–4°C until used unless otherwise specified. Experiments were carried out not later than 2¼ h after bleeding. For a prefusion heat treatment, erythrocytes were exposed by placing 0.5 ml of the cell suspension in a 40°C, 45°C, or 50°C waterbath for 20 min before transfer to the observation chamber. Control cells did not receive the heat treatment but were kept at 0–4°C until transfer to the observation chamber. Heat treatment experiments were performed at a chamber temperature of 20°C.

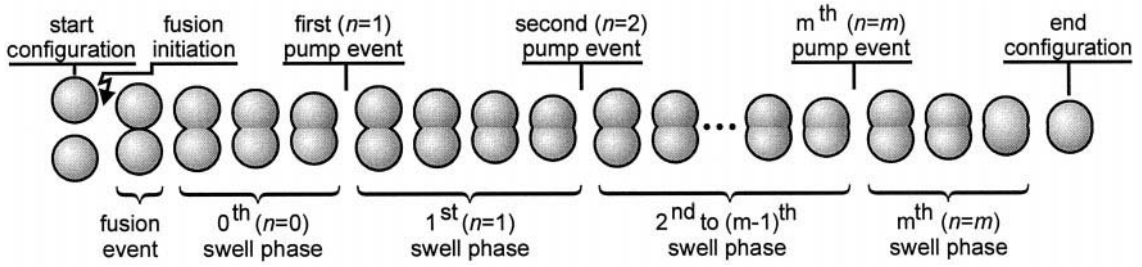

FIGURE 2 Definition of the terminology of all swell phases and pump events of an oscillating doublet. Because of its shape, the configuration at the beginning of a swell phase is termed the 8′-configuration, and that at its end is the O-configuration. The 0th swell phase shows the normal cell fusion kinetics. For reasons of clear graphing, the amplitudes of the changes have been exaggerated and the changes in the diameters of both cells have been omitted.

Fusion apparatus

The fusion chamber used for the experiments is an extension of that used by Baumann and Sowers (1996a), allowing four experiments with one single-chamber assembly. A small glass coverslip, a parafilm cut (American Can Company), and a square-sized glass slide were sandwiched together as shown in Fig. 4. This configuration was bonded together by heating and moderately melting the parafilm. Chambers were stored dust free until used.

For each experiment, one of the four chambers was filled by dispensing solution from a pipette tip from an opening on one side. The chamber instantly filled by capillary forces. Two platinum electrodes (1 mm in width and 100 μm in height with rounded tips) were introduced into the two openings of the filled chamber by a micropositioning device (Baumann and Grebe, 1998). Both electrodes were in contact with the solution and were adjusted to a distance of 1 mm. Afterward, the set of microchamber and electrodes was positioned on the stage plate of a noninverse microscope, where it was held securely in place by a magnet lock. After use, the chamber was disassembled and the glass slide cleaned for reuse.

The micropositioning device carrying the microchamber was fitted with two Peltier elements and a temperature measurement system with a feedback loop, thus allowing us to regulate the chamber temperature in the range between 0.5°C and 50.0°C with an accuracy of approximately ±0.5°C. Equilibration time needed for the mounted microchamber to reach the desired temperature was always below the time needed between the assembly on the microscope stage plate and the beginning of the measurement.

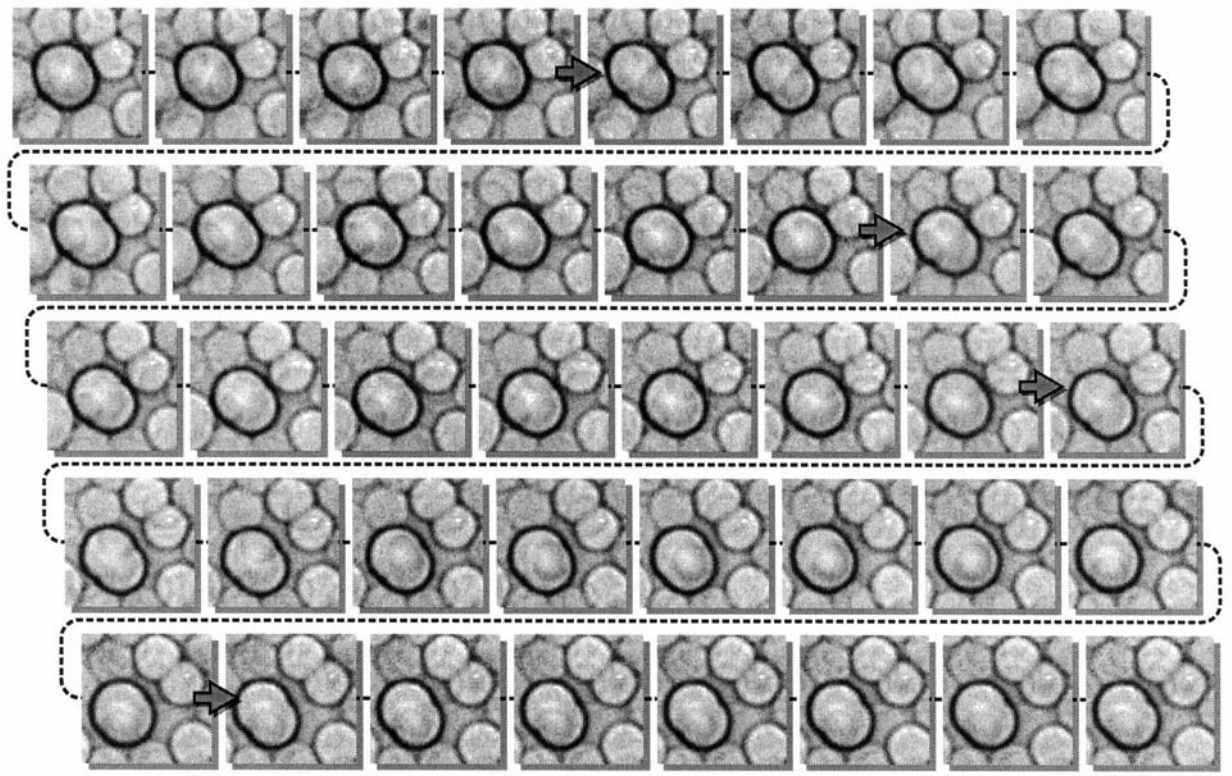

FIGURE 3 Sequence of images showing a doublet (*dark contours*) that undergoes an oscillatory movement. The sequence starts at the upper left image and proceeds to the image in the lower right corner. The time interval between two consecutive images is 5 s. The gray arrows indicate that in the interval a pump event motion has taken place. The oscillating doublet is surrounded by other fused and unfused erythrocytes of the cell monolayer, which, because of hemolysis, turned to ghosts and therefore showed less optical contrast. Although the two cells were of the same size before the fusion event (not shown), the doublet's spheres have different diameters, which clearly can be seen in the images after each pump event.

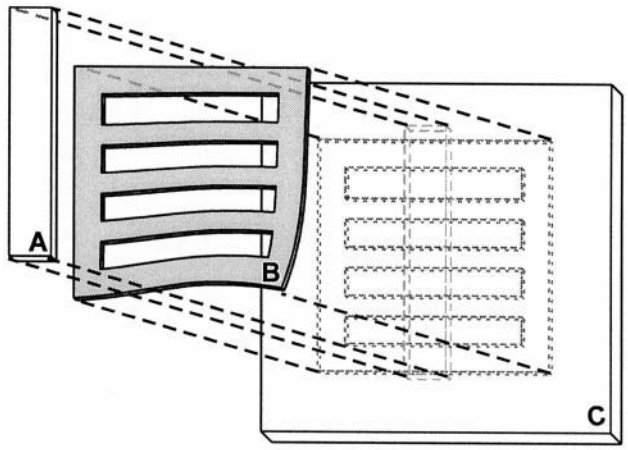

FIGURE 4 Sandwich assembly of the observation chamber. The top element is a glass coverslip (*A*) cut to 3 mm × 18 mm, lying on a parafilm slide (*B*) with four rectangular holes, each 2 mm × 12.5 mm. The parafilm is centered on a glass slide (*C*) with dimensions 25.4 mm × 25.4 mm × 1 mm. Moderate heating on a hot plate sealed the parafilm against both attached glass surfaces, giving four observation chambers, in each of which two electrodes could be inserted after they were filled with the blood sample. After a set of four experiments, parts were taken apart and the glass slide (*C*) was cleaned for reuse.

Fusion and oscillation protocol

Erythrocytes in their discocyte shape were allowed to settle on the bottom glass slide to form an almost continuous cell monolayer (Fig. 5, 0:00 to 2:45 min). After this, a series of three voltage pulses was applied to the cell monolayer (Fig. 5, 3:00 min, 3:30 min, and 5:00 min). The identical pulses had a close to rectangular shape, with an amplitude of 800 ± 20 V and a duration of 100 ± 2 μs and thus resulted in an electrical field strength of 8 kV/cm, calculated from an 800-V pulse amplitude divided by the 1-mm electrode spacing. The rectangular pulse shape was acquired by using only the first part of a capacitor discharge curve, where on and off switching of the curve was performed by field-effect transistors in a homemade pulse generator. The influence of the pulse amplitude on the number of oscillation cycles could be neglected (Baumann and Sowers 1996a).

After application of the first pulse (Fig. 5, 3:00 min), the shape of the cells changed to echinocytes because of pulse-induced reorientation of endofacial aminophospholipids to the outer leaflet of the bilayer (Henszen et al., 1997). The application of the second pulse (Fig. 5, 3:30 min) caused the cells to swell by osmotically driven forces to reach spherical shapes. The spherocytes were not fixed to the glass slide, which was verified by applying a moderate unidirectional buffer flow, resulting in a shear force and instantaneous movement of all spherocytes in the direction of the flow. At this point, a minor part of the cells showed hemolysis, resulting in a fading image of the cell contours. Some of these cells showed jumplike motions or "jumps" during the hemolysis, as recently described (Zade-Oppen, 1998), although no ejection of a cloud was detected. After the third pulse was applied to the monolayer (Fig. 5, 5:00 min), there was initially a high rate of hemolysis, covering typically 75% of all cells. The major part of the unhemolyzed cells underwent a fusion process with a neighbor cell that had physical membrane contact. The orientation of the fusion products was always parallel to the direction of the electric field (Baumann, 1998). All fusion products were of the "open-lumen" fusion type. The time of membrane and cell fusion was not exactly predictable; it was observed up to 30 s after the initiation of the third pulse.

The measurement period lasted from the third pulse up to the cessation of all oscillatory movement of the doublets. Fusion products were easily detected because of their high optical contrast, which was due to the remaining content of hemoglobin. Cells were observed and measured midway between the two electrodes, because there 1) the change in pH due to electrolytic reasons (Potter, 1988) was expected to be minimal and 2) the homogeneity of the electrical field distribution had a maximum (Baumann, 1998).

Two systems for image recording were in use. With the slow speed system, microscopic images taken by a PAL-TV CCD camera with a time resolution of 40 ms were recorded on videotape with a standard Umatic VCR (Sony, Japan). The tape was started before the third pulse and was not stopped before the observed doublets ceased to oscillate. A continuously running video timer alphanumeric signal was inserted on the screen to provide time information. Fast geometrical shape changes were recorded by a digitally operating high-speed CCD camera (MD4256; Reticon, Sunnyvale, CA) acquiring 1000 frames/s unless otherwise specified. The high-speed images were recorded in a 2048-image memory buffer installed in a standard PC. Each image had 256 × 256 pixels with an 8-bit gray-scale resolution. Posttriggering facilities of the camera's software were used to evaluate 50 consecutive images (10 before the pump event and 40 after) of each pump event.

Calculation of membrane area and doublet volume

Because a doublet can be geometrically modeled as two intersected spheres (see Fig. 6), it is possible to calculate both the membrane surface area A and the doublet volume V from the measurement of three geometrical values: the radii r_1, r_2 of the spheres and the distance d_{12} between their center points. Where h_1 and h_2 are the length of the doublet's symmetry axis from the pole to the fusion zone (see Fig. 1) within sphere 1 or sphere 2, respectively,

$$h_1 = \frac{(r_1 + d_{12})^2 - r_2^2}{2 \cdot d_{12}} \quad \text{and} \quad h_2 = \frac{(r_2 + d_{12})^2 - r_1^2}{2 \cdot d_{12}} \tag{1}$$

one can access the membrane surface area A and the doublet volume V with the following equations (Baumann, 1998):

$$A = 2\pi(r_1 \cdot h_1 + r_2 \cdot h_2) \tag{2}$$

$$V = \frac{\pi}{3}\left[h_1^2 \cdot (3 \cdot r_1 - h_1) + h_2^2 \cdot (3 \cdot r_2 - h_2)\right] \tag{3}$$

The relative volume change ∂V of doublets before and after a pump event of a swell phase was calculated based on of the calculated volumes V:

$$\partial V = \frac{V_{\text{after}} - V_{\text{before}}}{V_{\text{before}}} \tag{4}$$

During a pump event, ∂V is negative because of the sudden volume loss caused by a membrane rupture and visible in the jet. During a swell phase, ∂V is positive because of the colloid osmotic volume increase in the doublet (Baumann, 1998).

The images of the camera records provided an optical resolution of 0.42 μm. A homemade software image analysis tool, based on an adapted Hough transformation, was used to extract the three primary values from each bitmap image. Because the camera images contained optical and thermal noise, the plotted curves of the primary data did not exhibit smooth changes with time (see Fig. 7, *gray lines* in diagrams for r_1, r_2, and d_{12}), resulting in noisy plots for the calculation results of A and V. Therefore, a curve fit algorithm was applied to the primary data (Fig. 7, *black lines* in diagrams for r_1, r_2, and d_{12}) before the membrane surface area A and the doublet volume V were calculated based on the values of these fit functions (Fig. 7, diagrams for A and V).

Pump event parameter measurement

To acquire pump event parameters, the fit function for the pump event was chosen to be a combination of a constant value r_0 before the beginning of

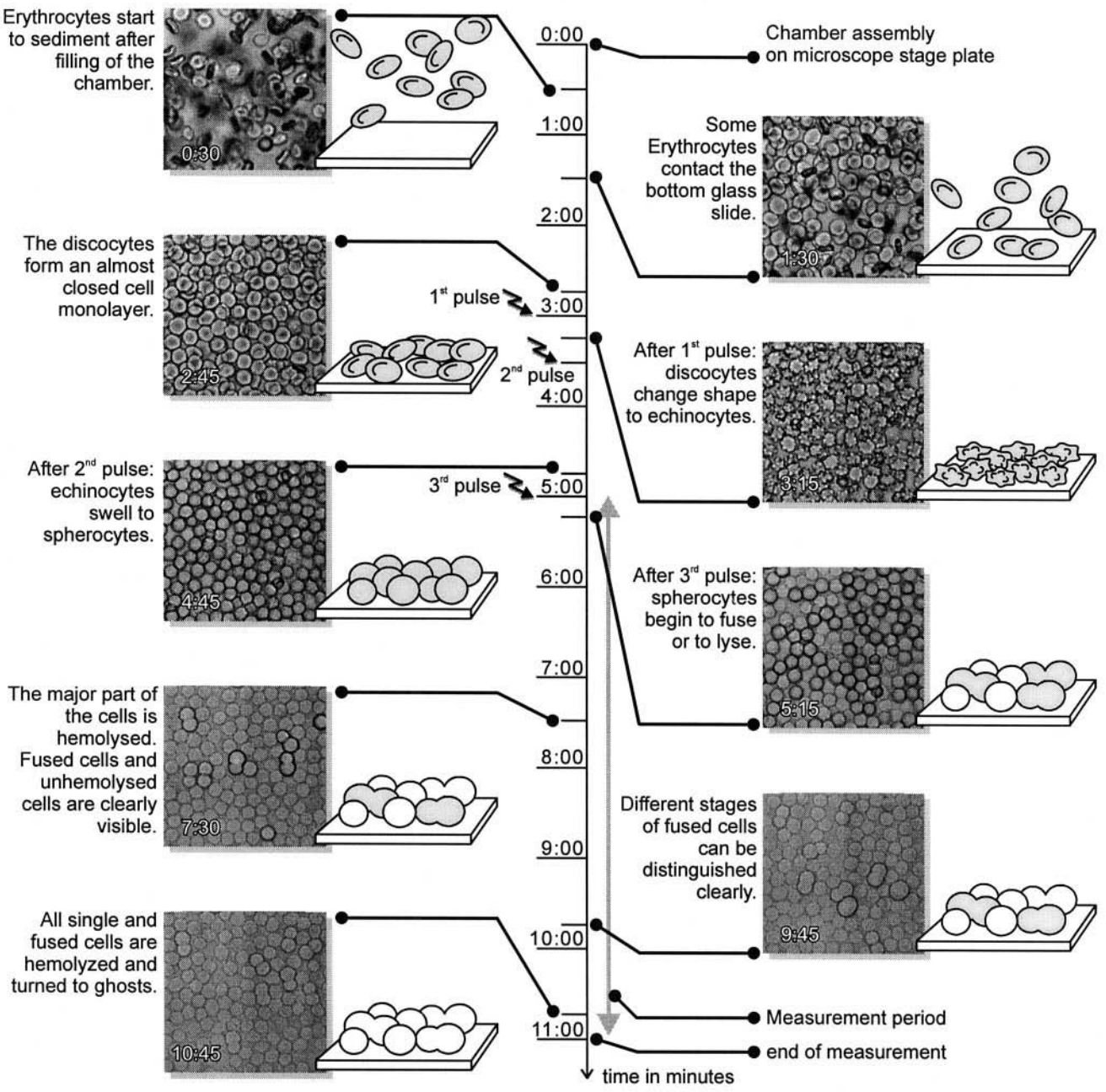

FIGURE 5 Fusion protocol applied to the erythrocyte monolayer to reach high yields of oscillating doublets. The time line shows, from top to bottom, light microscopic images of the cells and an illustration of how the cells assembled on the bottom glass slide. Three voltage pulses were applied to the cell monolayer: the first caused the then discocytes to change shape to echinocytes, the second caused a shape change to spherocytes by colloid osmotic swelling, and the third initiated fusion and oscillation therewith. The measurement period started after the third pulse and lasted until the doublet(s) observed ceased to show an oscillating movement (11:00 min in the example shown).

the pump event ($t_0 = 0$ ms) and an exponentially increasing or decaying function toward the end value of r_∞ afterward, starting from the constant value r_0, as shown in Fig. 7 *A* and given in Eq. 5:

$$r_{\text{fit}}(t) = \begin{cases} r_0 & \text{for } t < t_0 \\ r_0 - (r_0 - r_\infty) \cdot e^{(t - t_0)/\tau} & \text{for } t \geq t_0 \end{cases} \quad (5)$$

The amplitude of each geometrical change thus can be calculated with $|r_\infty - r_0|$, and the time constant of the pump event is given through τ. A complete example of a doublet's first pump event is shown in Fig. 7 *A*. The fit functions (Fig. 7 *A*, *black lines* in the diagrams of the top row) fit the corresponding acquired data reasonably well (*gray lines*). Because the signal-to-noise ratio of the measurements of d_{12} was always bigger than that of r_1 or r_2, the fit to d_{12} was always the most accurate, and therefore the time constant τ was defined by the fit function $d_{12,\text{fit}}$.

Swell phase parameter measurement

The fit function for the swell phases was the sawtooth function given in Eq. 6. Its time course is shown in Fig. 7 *B* (*top three graphs*). Analogously to the pump event parameter calculation, the values of the fitted functions for

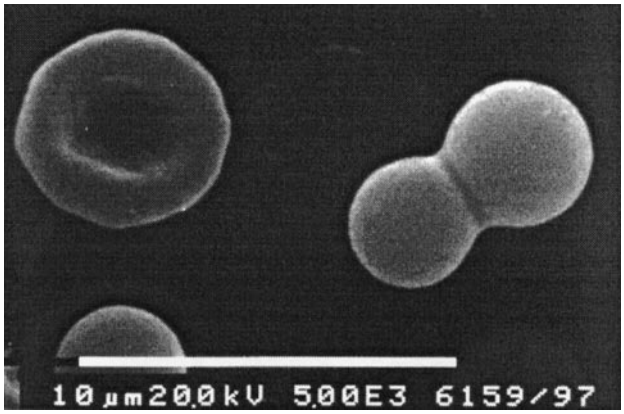

FIGURE 6 Electron microscopic image of an discocyte (*left*) and a doublet (*right*). After the oscillation protocol, cells were treated with 1.5% glutaraldehyde solution to fix cell membranes. Clearly visible are the circular shapes and the different sizes of both spheres of the doublet. The smooth fusion zone observable between the doublet's two spheres is due to the membrane shrinkage after the glutaraldehyde treatment. The white bar represents a length of 10 μm.

r_1 or r_2 and d_{12} have been the basis for calculation of membrane surface area A and doublet volume V (Fig. 7 *B, bottom two graphs*). In the definition of the sawtooth function,

$$r_{\text{fit}}(t) = \begin{cases} r_{0e} & \text{for } t < t_1 \\ \dfrac{r_{1e} - r_{1b}}{t_2 - t_1} + \left(r_{1b} - \dfrac{r_{1e} - r_{1b}}{t_2 - t_1} \cdot t_1 \right) & \text{for } t_1 \le t < t_2 \\ \dfrac{r_{2e} - r_{2b}}{t_3 - t_2} + \left(r_{2b} - \dfrac{r_{2e} - r_{2b}}{t_3 - t_2} \cdot t_2 \right) & \text{for } t_2 \le t < t_3 \\ \dfrac{r_{3e} - r_{3b}}{t_4 - t_3} + \left(r_{3b} - \dfrac{r_{3e} - r_{3b}}{t_4 - t_3} \cdot t_3 \right) & \text{for } t_3 \le t < t_4 \\ r_{4b} & \text{for } t_4 \le t \end{cases} \quad (6)$$

the numerical indices to t name the ordinal number of the pump events (1–4), the numerical indices to r name the ordinal number of a swell phase, the alphabetical index b names the beginning of a swell phase, and the alphabetical index e names the end of the swell phase, according to Fig. 2.

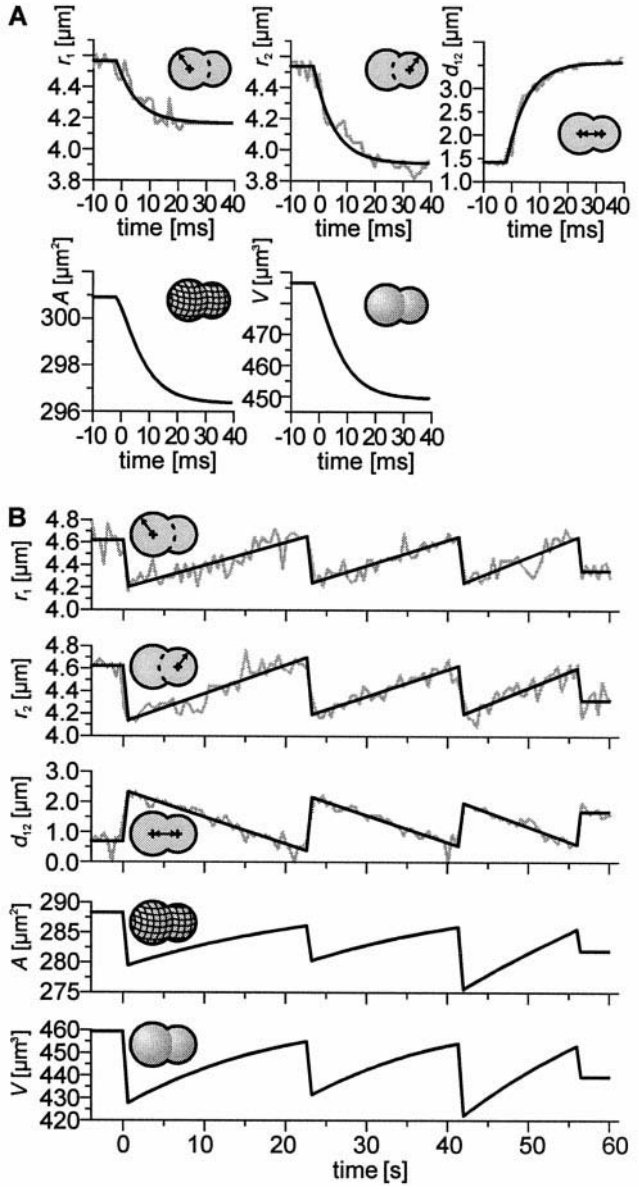

FIGURE 7 Example of the measurement of r_1, r_2, and d_{12} during the first pump event (*A*) and during the first to third swell phases (*B*) of a doublet (*gray lines*) and the results of the constant-to-exponential fits (*A*) and of the sawtooth fits (*B*) $r_{1,\text{fit}}(t)$, $r_{2,\text{fit}}(t)$, and $d_{12,\text{fit}}(t)$ to these values (*black lines*). The calculations of the membrane surface area A and doublet volume V (two bottom diagrams in *A* and *B*) are based on the values given by the fit functions. (*A*) The time $t = 0$ ms was defined when the pump event started. The decrease in membrane surface area A and doublet volume V is almost exponential in time. The time constant for the pump event shown is $\tau = 7.7$ ms. (*B*) The time $t = 0$ s was defined when the first swell phase started. The increase in membrane surface area A and doublet volume V is not linear and slows down close to the end of each of the three swell phases.

RESULTS

General and long time observations

The average membrane area increase during the swell phase until membrane rupture was 3.2 ± 2.1% and matches the data acquired with micropipette aspiration of 3.0 ± 0.7% (Evans et al., 1976). The narrowing at the fusion zone area was visible during the whole oscillation cycle by a darker line. Only shortly before the pump events took place, the fusion zone's optical contrast faded slightly. The relation between doublet length and fusion-zone diameter was always close to 1.136 before a pump event occurred.

No linear or even monotonic behavior in the development of swell phases during the oscillation cycle could be detected (see Fig. 8 and Baumann and Grebe, 1998). Swell phase durations ranged from 0.5 s up to more than 3 min, showing neither a continuously growing duration nor a continuously shrinking duration. Most of the oscillating doublets showed that with an ongoing oscillation process the length of the swell phases became shorter. Most of the doublets that were evaluated showed a decrease in all geometrical amplitude changes with proceeding oscillation time.

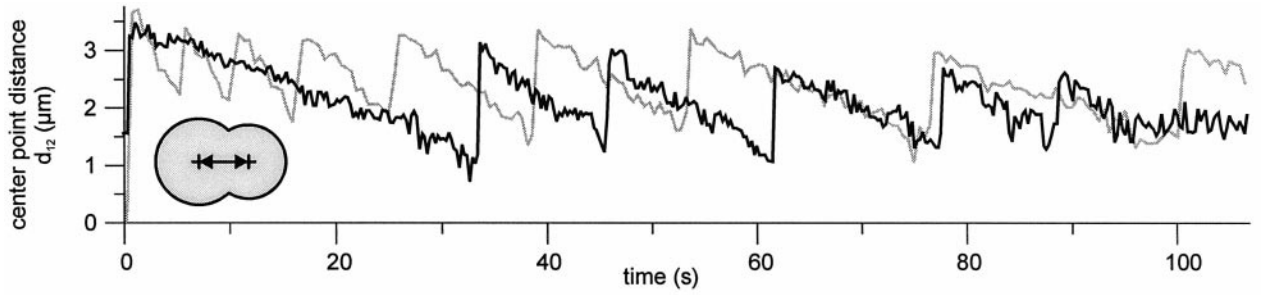

FIGURE 8 Dynamics of the first swell phases of two doublets, shown as the time course of the center point distance d_{12}. Both time scales start with the first pump events. The oscillation history of one doublet (*black line*) is such that swell times almost continuously decrease with ongoing oscillation. After ~100 s and six swell phases, the oscillation ceased. The oscillation history of the other doublet (*gray line*) differed because 1) swell phase periods increased with time and 2) the oscillation went on after the end of recording at 108 s.

Nearly all oscillating doublets showed asymmetrical sizes of the spheres after some oscillation cycles (Figs. 3 and 6). This observation of a unilateral shift in size was visible not only with doublets, but also with cell clusters of three (triplets) to six cells (not shown). During the final oscillation cycles, all oscillating doublets underwent only minimal geometrical changes, close to the border of detection.

The transition between the pump event motion and the swell phase motion is smooth (Fig. 9) and can be linearized as late as 200 ms after the pump event. Evaluation of multiple transitions showed that the pump event time constant τ could be accessed safely from the fit function shown in Eq. 5 by applying it to a data set starting 10 ms before the pump event and ending 40 ms after (Baumann, 1998).

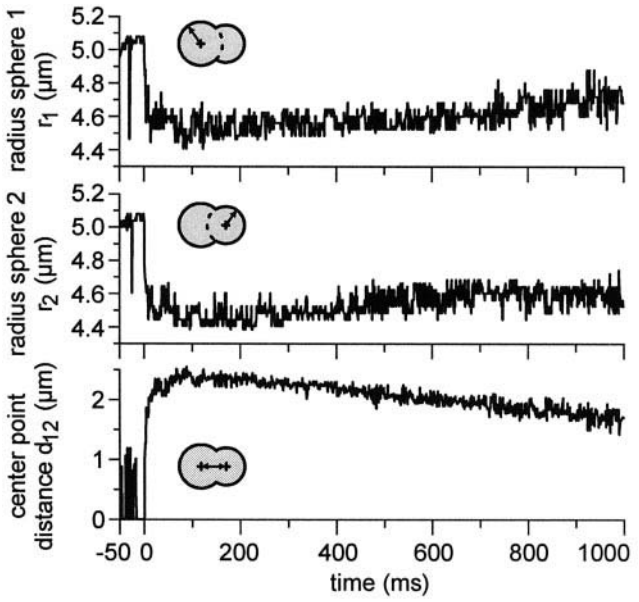

FIGURE 9 The transition of a pump event into the swell phase shown with data from r_1, r_2, and d_{12}. With the beginning of the pump event the time scale was set at 0 ms. The exponential development of all three time courses in approximately the first 40 ms shows a continuous shift toward linear functions. Time resolution was set at 2 ms. The downward showing peaks in the r_1 and r_2 data at −30 ms and −24 ms, respectively, are due to a failure of the automatic contour detection.

Chamber temperature and heat treatment influence

The time constant τ of the first pump event was measured at four different chamber temperatures. The results (Fig. 10 *A*, *squares*) show that with increasing chamber temperature the average pump event time constant τ decreased from 5.5 ms to 3.8 ms (69% of the initial value). The influence of an increasing chamber temperature on the decrease in swell time duration is weak but significant (Fig. 10 *A*, *circles*).

Neither the relative volume decrease during the pump events nor the relative volume increase during the swell phases depended significantly on chamber temperature (Baumann, 1998). The relative volume change averaged for all investigated chamber temperatures decreased from $-7.3 \pm 4.6\%$ to $-5.5 \pm 3.2\%$ from the first to the second pump event, and from $8.7 \pm 4.4\%$ to $3.2 \pm 2.2\%$ from the first to the second swell phase ($N = 64$ doublets for each data value).

A heat treatment of 40°C and 45°C had no significant influence on the time constants or on the swell times of doublets (Fig. 10 *B*, *squares* and *circles*). The relative volume changes between the first and the second pump events or swell phases decreased slightly, but not significantly, from $-7.4 \pm 4.5\%$ to $-5.9 \pm 3.1\%$ and from $9.2 \pm 4.0\%$ to $7.4 \pm 4.5\%$, respectively ($N = 34$ doublets for each data value). These results have been averaged for control cells and the cells that received a heat treatment of 40°C and 45°C because there was no difference in the relative volume changes within either of these groups. After a heat treatment of 50°C, erythrocyte fusion was possible, but none of the fused doublets showed oscillatory movements. Shapes of the doublets were irregular.

Fusion types were "open-lumen" fusions for all doublets, independently of the temperature of heat treatment.

Jet characteristics

The jet, the image of an ejection of endoplasmic volume, was visible as a light-gray cloud close to the membrane,

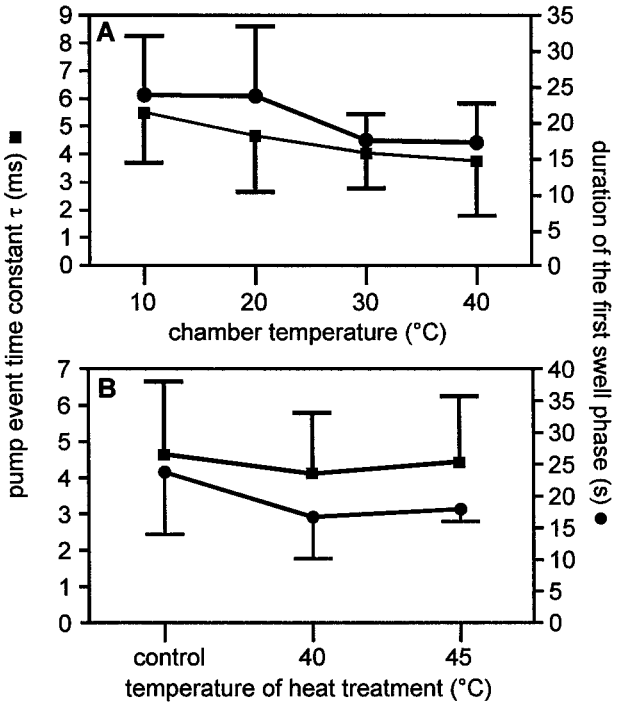

FIGURE 10 Development of time constants (■) and swell times (●) with increasing chamber temperature (*A*) and as a function of heat treatment (*B*). (*A*) The time constant τ of the first pump event of doublets decreases significantly with increasing chamber temperature in the range between 10°C and 40°C (number of measurements: $N = 14$ doublets for each data point), and the durations of the first swell phases also decrease, though not constantly, with increasing chamber temperature ($N = 16$ doublets for each data point). (*B*) The time constant of the first pump event is not affected by a heat treatment up to 45°C for 20 min ($N = 12$ doublets for each data point). Because the values for the relative volume change ∂V of the first to third swell phases did not vary for each heat treatment investigated, each data point shows a combination of the first to third swell phase values. They show no dependency on the heat treatment temperature ($N_{control} = 14$ doublets, $N_{40°C} = N_{45°C} = 10$ doublets). Data from doublets with heat treatment 50°C, 20 min are not shown because this heat treatment caused the oscillation to disappear.

occurring in a time below 1 ms and vanishing within several milliseconds. A jet was clearly visible if it emerged from the rim of the doublet contour, as shown in Fig. 11, *B* and *C*. Jets were less visible if they emerged from the doublet's top in the direction of the light path (Fig. 11 *D*), and they were unobservable if they emerged toward the bottom glass slide. Because each oscillating doublet that was observed never showed more than a single jet at a time, the number of membrane ruptures after the membrane area expansion can be limited to one. When emerging from the rim of the doublet contour, 66.6% of the jets pointed toward the anode and 16.7% pointed toward the kathode. The remaining 16.7% of the jets pointed perpendicular to the electric field lines, neither toward the anode nor toward the cathode. The kinetic energy of a single jet is sufficient to induce a dislocation of a neighboring ghost on the bottom glass slide (Fig. 11). There was a 54% to 46% distribution of jets emerging from the bigger sphere or from the smaller sphere, respectively.

DISCUSSION

The oscillation of electrofused erythrocyte doublets is a phenomenon governed in its time courses by both the physical properties of the suspension medium and the biological properties of cell membranes.

The characteristics of the oscillation cycles of electrofused doublets, as far as they have been evaluated in this study, show a dependency of the chamber temperature and, up to a heat treatment of 45°C, no dependency of the heat treatment temperature. A heat treatment of more that 49.5°C for at least 10 min is known to cause a spectrin denaturation (Brandts et al., 1977) and thus affects mechanical membrane properties. After the cells have been exposed to the 50°C heat treatment procedure, the oscillatory movement of the doublets was undetectable because of denaturation of the membrane skeleton. The viscosity of Newtonian fluids is known to decrease with increasing temperature, and unheated hemoglobin solutions can be treated as Newtonian fluid (Müller et al., 1992). Because of this, the decrease in the time constant τ with increasing chamber temperature (Fig. 10 *A*, *squares*) can be explained with the decrease in cytosolic viscosity that enables the jet to emerge faster through the membrane rupture. Because the volume increase during the swell time is due to colloid osmotic forces, solute and water diffusion through the membrane is faster at higher temperatures and thus can be a cause of the lower swell times observed (Fig. 10 *A*, *circles*). This work is not necessarily in contradiction to the observation that a heat treatment of 42°C for 20 min causes a change from a "flat diaphragm" to an "open lumen" fusion (Sowers et al., 1994) because even cells that received no heat treatment never showed a "flat diaphragm" fusion. This, in turn, may be caused by the different fusion protocols used.

At least two possible explanations can be given for the decrease in the relative volume changes between the first and second pump events and between the first and second swell phases: 1) there may have been a gradual decrease in membrane area due to membrane vesiculation, and 2) there may have been been a gradual loss of membrane elasticity during the oscillation period, which possibly causes weaker elastic forces to be stored in the membrane. Because a decrease in the doublet's membrane area could not be measured, it is assumed that elastic membrane properties are subject to change during the oscillation cycle. Furthermore, after the first pump event has taken place, the membrane may show a weakening at the rupture site, which causes the rupture to occur earlier and therefore at a smaller relative volume increase.

The result that 66.6% of all jets observed are directed toward the anode supports earlier findings (Mehrle et al., 1989; Teissié and Rols, 1993) that the critical potential difference that induces membrane electropermeabilization is located where the membrane points toward the anode.

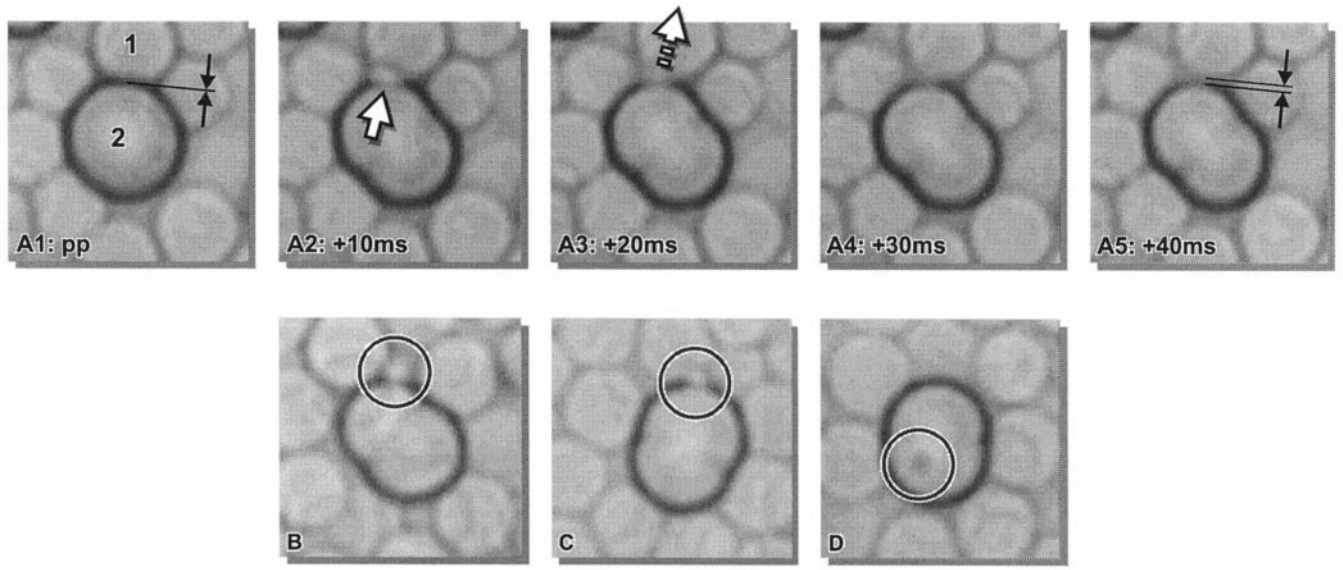

FIGURE 11 (*A1–A5*) Sequence of images of the first pump event of a single doublet. In the last prepump event image (*A1*: pp), a ghost (*1*) is located in close membrane contact to the doublet (*2*), but is unfused. The image *A2*, 10 ms later, shows that a jet leaves the doublet close to the contact site of cells 1 and 2, dislocating ghost 1. The last image, *A5*, 40 ms after the first, shows that the ghost moved ~1 μm through the kinetic energy of the jet. (*B–D*) Images taken during the first pump events of three different doublets; each image was taken 4 ms after the beginning of the pump event. All images show a jet within the circle. In the images, the electric field direction is oriented vertically; the cathode is below and the anode is above the doublet images. (*B*) The jet emerges from the smaller sphere. (*C*) The jet emerges from the bigger sphere. In *B* and *C*, the membrane rupture points toward the anode. (*D*) The membrane rupture points perpendicular to the electric field. Before the pump events, the spheres of all doublets shown were of almost identical size.

The dislocation of swollen erythrocytes due to small forces like a jet (Fig. 11 *A*) was reported recently (Zade-Oppen, 1998) and can occur because the cells are not attached to the bottom glass slide. The jet itself should always emerge from the bigger sphere because the membrane tension of a sphere depends linearly on the pressure difference across the membrane and on the sphere's radius (Jay and Canham, 1977). This was not observed, and therefore it that can be concluded that the mechanical influence of the jet location is less important than an electrically induced membrane permeabilization.

The intracellular spectrin cytoskeleton can be described as a triangular network (Boal, 1994; Steck, 1989). The fusion zone expansion during the fusion process strongly depends on the presence of the cytoskeleton and is increased when spectrin is denaturated (Sowers et al., 1994). Because of this it is assumed that the deformation of spectrin in the fusion zone area is responsible for the persistence of the narrowing in the fusion zone area during the oscillation cycles, as schematically drawn in Fig. 12. Then during fusion zone expansion, the spectrin tetramers parallel to the fusion zone are elongated more than those perpendicular to the fusion zone (Fig. 12, *from left to right*). To fit this model, the spectrin cytoskeletons of both cells do not necessarily have to be fused like the lipid bilayers, but because there has been a unilateral shift in the size of the spheres there must have been a unilateral shift of lipid bilayer across the fusion zone, and it is likely that the parts of the spectrin cytoskeleton also followed this shift. The anisotropic deformation of the spectrin in the fusion zone may cause an increased rigidity to further expansion, indicating that the fusion zone possesses a comparably high elasticity modulus (Baumann, 1998) and thus may cause it to remain visible during the oscillation process.

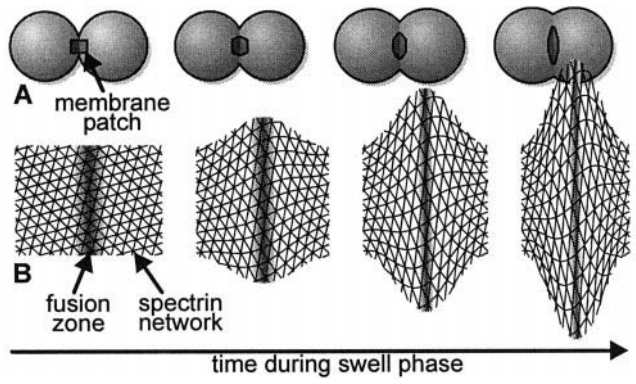

FIGURE 12 Hypothetical model of how the persistence of the narrowing in the fusion zone area during the oscillation process can be explained. (*A*) A schematic drawing of a doublet undergoing fusion kinetics, i.e., continuous growth of the fusion zone diameter. A rectangular membrane patch close to the fusion zone, drawn on the first doublet, is likely to deform as shown. (*B*) A zoom into each of the four patches, giving the deformation of the intracellular triangular spectrin network. Because the vertical elongation (i.e., the direction of the fusion zone drawn here) of the membrane patch during the fusion process is bigger than the horizontal change in length, all vertical running spectrin tetramers may soon approach the maximum possible elongation, after which an increase in length is impossible without tetramer rupture. Thus the fusion zone's elongation modulus possibly increases and the narrowing remains visible.

REFERENCES

Akkaş, N. 1984. Biomechanics of virus-to-cell and cell-to-cell fusion. *J. Biomed. Eng.* 6:257–264.

Baumann, M. 1998. Untersuchungen zur zyklischen Formänderung elektrofusionierter Erythrozyten. Dissertation, RWTH Aachen.

Baumann, M., and R. Grebe. 1998. Characteristics of the osmotically induced membrane rupture. *Mol. Membr. Biol.* 15:193–201.

Baumann, M., and A. E. Sowers. 1996a. A mechanical cycling phenomenon in electrofused erythrocytes. *Mol. Membr. Biol.* 13:113–119.

Baumann, M., and A. E. Sowers. 1996b. Membrane skeleton involvement in cell fusion kinetics: a parameter that correlates with erythrocyte osmotic fragility. *Biophys. J.* 71:336–340.

Brandts, J. F., L. Erickson, K. Lysko, A. T. Schwartz, and R. D. Taverna. 1977. Calorimetric studies of the structural transitions of the human erythrocyte membrane. The involvement of spectrin in the A transition. *Biochemistry.* 16:3450–3454.

Boal, D. H. 1994. Computer simulation of a model network for the erythrocyte cytoskeleton. *Biophys. J.* 67:521–529.

Chernomordik, L. V., and A. E. Sowers. 1991. Evidence that the spectrin network and a nonosmotic force control the fusion product morphology in electrofused erythrocyte ghosts. *Biophys. J.* 60:1026–1037.

Evans, E. A., R. Waugh, and L. Melnik. 1976. Elastic area compressibility modulus of red cell membrane. *Biophys. J.* 16:585–595.

Glaser, R. W., and E. Donath. 1987. Hindrance of red cell electrofusion by the cytoskeleton. *Stud. Biophys.* 121:37–43.

Henszen, M. M. M., M. Weske, S. Schwarz, C. W. M. Haest, and B. Deuticke. 1997. Electric field pulses induce reversible shape transformation of human erythrocytes. *Mol. Membr. Biol.* 14:195–204.

Hernandez, L. D., L. R. Hoffman, T. G. Wolfsberg, and J. M. White. 1996. Virus-cell and cell-cell fusion. *Annu. Rev. Cell Dev. Biol.* 12:627–661.

Jay, A. W. L., and P. B. Canham. 1977. Viscoelastic properties of the human red blood cell membrane. II. Area and volume of individual red cells entering a micropipette. *Biophys. J.* 17:169–178.

Knutton, S., and C. A. Pasternak. 1979. The mechanism of cell-cell fusion. *Trends Biochem. Sci.* 4:220–223.

Lentz, B. R. 1994. Polymer-induced membrane fusion: potential mechanism and relation to cell fusion events. *Chem. Phys. Lipids.* 73:91–106.

Marsden, N. V. B., A. M. M. Zade-Oppen, and H. G. Davies. 1981. Jet expulsion of cellular contents from red cells during photodynamic hemolysis. *Ups. J. Med. Sci.* 86:1–8.

Mehrle, W., R. Hampp, and U. Zimmermann. 1989. Electric pulse induced membrane permeabilisation. Spatial orientation and kinetics of solute efflux in freely suspended and dielectrophoretically aligned plant mesophyll protoplasts. *Biochim. Biophys. Acta.* 978:267–275.

Montane, M.-H., E. Dupille, G. Alibert, and J. Teissié. 1990. Induction of a long-lived fusogenic state in viable plant protoplasts permeabilized by electric fields. *Biochim. Biophys. Acta.* 1024:203–207.

Morris, S. J., D. P. Sarkar, J. M. White, and R. Blumenthal. 1989. Kinetics of pH dependent fusion between 3T3 fibroblasts expressing influenza hemagglutinin and red blood cells. Measurement by dequenching of fluorescence. *J. Biol. Chem.* 264:3972–3978.

Müller, G. H., H. Schmid-Schönbein, and H. J. Meiselman. 1992. Development of viscoelasticity in heated hemoglobin solutions. *Biorheology.* 29:203–216.

Pohl, H. A. 1978. Dielectrophoresis. Cambridge University Press, Cambridge.

Potter, H. 1988. Electroporation in biology: methods, application and instrumentation. *Anal. Biochem.* 174:361–373.

Schmid-Schönbein, H. 1996. Physiological synergetics: a holistic concept concerning phase jumps in the behaviour of driven nonlinear systems. *In* Comprehensive Human Physiology. R. Greger and U. Windhorst. Springer-Verlag, Berlin and New York. 43–68.

Song, L., Q. F. Ahkong, D. Georgescauld, and J. A. Lucy. 1991. Membrane fusion without cytoplasmatic fusion (hemi-fusion) in erythrocytes that are subjected to electrical breakdown. *Biochim. Biophys. Acta.* 1065: 54–62.

Sowers, A. E. 1987. The long-lived fusogenic state induced in erythrocyte ghosts by electric pulses is not laterally mobile. *Biophys. J.* 52: 1015–1020.

Sowers, A. E. 1990. Low concentrations of macromolecular solutes significantly affect electrofusion yield in erythrocyte ghosts. *Biochim. Biophys. Acta.* 1025:247–251.

Sowers, A. E. 1992. The role of both postfusion lumen expansion and membrane fusion in the entry of cells by enveloped viruses. *Membr. Interactions.* 203–214.

Sowers, A. E. 1995. Membrane skeleton restraint of surface shape change during fusion of erythrocyte membranes: evidence from use of osmotic and dielectrophoretic microforces as probes. *Biophys. J.* 69:2507–2516.

Sowers, A. E., J. D. Rosenberg, and Y. Wu. 1994. Membrane electrofusion: a paradigm for study of membrane fusion mechanisms. *In* Charge and Field Effects. M. J. Allen, S. F. Cleary, and A. E. Sowers, editors. World Scientific Publishing, River Edge, NJ. 403–419.

Steck, T. L. 1989. Red cell shape. *In* Cell Shape: Determinants, Regulation and Regulatory Role. W. Stein and F. Bronner, editors. Academic Press, New York. 205–246.

Steubing, R. W., S. Cheng, W. H. Wright, Y. Numajiri, and M. W. Berns. 1991. Laser induced cell fusion in combination with optical tweezers: the laser cell fusion trap. *Cytometry.* 12:505–510.

Teissié, J., and M. P. Rols. 1993. An experimental evaluation of the critical potential difference inducing cell membrane electropermeabilization. *Biophys. J.* 65:409–413.

Wu, Y., J. G. Montes, and R. A. Sjodin. 1992. Determination of electric field threshold for electrofusion of erythrocyte ghosts. *Biophys. J.* 61: 810–815.

Wu, Y., J. D. Rosenberg, and A. E. Sowers. 1994a. Surface shape change during fusion of erythrocyte membrane is sensitive to membrane skeleton agents. *Biophys. J.* 67:1896–1905.

Wu, Y., R. A. Sjodin, and A. E. Sowers. 1994b. Distinct mechanical relaxation components in pairs of erythrocyte ghosts undergoing fusion. *Biophys. J.* 66:114–119.

Zade-Oppen, A. M. M. 1998. Repetitive cell "jumps" during hypotonic lysis of erythrocytes observed with a simple flow chamber. *J. Microsc.* 192:54–62.

Zimmermann, U. 1982. Electric field-mediated fusion and related electrical phenomena. *Biochim. Biophys. Acta.* 694:227–277.

Zimmermann, U., and J. Vienken. 1982. Electric field induced cell-to-cell fusion. *J. Membr. Biol.* 67:165–182.